Impact parameters and intraband scattering in electron diffraction from thin foils

1995 J. Phys.: Condens. Matter 7 803

(http://iopscience.iop.org/0953-8984/7/4/011)

J. Phys.: Condens. Matter 7 (1995) 803–809. Printed in the UK

Impact parameters and intraband scattering in electron diffraction from thin foils

A J Bourdillon

National University of Singapore, Department of Physics, Lower Kent Ridge Road, Singapore 0511

Received 8 July 1994, in final form 4 October 1994

Abstract. In transmission electron microscopy, Al core losses excited by currents localized about atomic cores show fringes similar to the thickness fringes observed in zero loss. The fringes observed in the inelastically scattered electrons result from intraband scattering in the dispersion of Bloch waves even when the losses are over 1 kV. The analysis uses dynamical scattering with inelastic scattering. The impact parameter method is used to determine transition rates from electron currents distributed across the unit cell of the crystal.

1. Introduction

Classical methods are being increasingly used to compute and understand such phenomena as electron capture (Ben-Itzhak *et al* 1993), screening in atomic collisions (Ricz *et al* 1993), molecular vibrational and rotational excitations (Celiberto and Rescigno 1993) and atomic transition rates (Burgess and Sheorey 1974). These methods generally employ simplifying approximations, which make it possible to conveniently calculate experimentally measurable quantities. The methods are particularly suitable for calculating averages in statistical distributions of multiple events since the uncertainties are less than is typical of individual events. Here the methods are applied to understand observed intraband scattering (Howie 1963) in high-loss inelastic scattering of fast electrons by crystals.

We have previously used such methods (Bourdillon 1984) to understand the influence of the impact parameter, b, in the Borrmann (1941) effect. This effect is encountered in x-ray and electron scattering as an increase in absorption when a beam is oriented, in the symmetric Laue condition, parallel to a set of diffracting planes, especially of low index planes (Hall 1966, Cherns *et al* 1973, Bourdillon *et al* 1981). The impact parameter is an unobservable in the Bethe (1930) scattering theory. The expectation value, $\langle b \rangle$, can be calculated, however, in semi-classical theory using mathematical 'cut off' devices (Burgess and Tully 1978, Burgess and Sheorey 1974). Reasonable estimates for the cut-off have been found to provide values for collision cross-sections consistent with values obtained by independent calculations, e.g. using the Bethe or Born theories.

The impact parameter method, using rectilinear orbits, is particularly suitable for describing the interactions due to a fast charged particle, especially when (i) this is described by a finite basis set of Bloch waves with defined momentum, k and (ii) energy losses at high scattering angle (as large as the Bragg angle) result in breaking of dipole selection (with unit change in angular momentum). In consequence, a basis set of spherical harmonics has reduced usefulness. This has been used in an alternative method, using partial waves with good angular momentum quantum numbers (Saldin and Rez 1987) for simple cases of

0953-8984/95/040803+07$19.50

small and large scattering vector. However, the method suffers an inherent disadvantage in complexity for computations involving continuous sets of Bloch waves, spread over a range of angles and energy losses. A more adequate result can be simply and transparently obtained by simulating, using standard methods, current distributions derived from elastic scattering (Howie 1963, Bourdillon *et al* 1981), and then calculating respective inelastic transition rates for these currents (Bourdillon 1984). The separation of inelastic from elastic effects is justified by the very different mean free paths when energy losses are high (> 50 eV) in a diffracting crystal.

2. Theoretical preliminaries

It is well known that the cross-section for large-angle scattering, as calculated by Rutherford through the impact parameter, provides the same answer as quantum mechanical calculations (Schiff 1968).

In the impulse approximation, inelastic transition rates can be calculated for scattering from either a stationary particle (Bohr 1913) (see the dashed line in figure 1) or from a bound state (Seaton 1962) (between the dotted lines in figure 1). The linear momentum distribution of the ground state causes an uncertainty in the final state wavevector, k_f as illustrated in the momentum diagram shown in figure 1 for an ionization of a core state. Notice that if the wavevector of the incident electron $k_i \gg \Delta k$, then Δk is approximately proportional to the energy loss. Then in this three-body interaction, the momentum transfer given to the fast electron, q, consists of three components: namely, the binding energy of a core state, the kinetic energy of the ionized electron, k_e, and the recoil of the excited atom, k_a.

Transition rates can be calculated by the impact parameter method (see, e.g., Burgess and Sheorey 1974) or by the more conventional Bethe theory (Bethe 1930, Bethe and Jackiw 1968, Inokuti 1971, Egerton 1986). These transition rates can be combined with separate elastic cross-sections (Doyle and Turner 1968, Geiger 1962) which dominate at both low and high angles (Reimer 1984). The mean impact parameter applicable to inelastic continuum transitions has been evaluated in various ways.

From the Heisenberg uncertainty principle, an energy loss event should be associated with a time interval corresponding to $\Delta\tau > \hbar/E$. If, for an inelastic collision with a rectilinear orbit, a typical impulse time is $\Delta\tau \approx b'/v$, then $b' > \hbar v/E$. When applied to electron scattering, as in the Borrmann effect, the theoretical parameter derived in this way, b', turns out to be large because the derivation does not take due account of the increasingly strong interaction that occurs with decreasing b. Thus, for example, in the ionization of an O 1s core electron by a 100 kV electron, the value $\pi b'^2$ has a value thirty times greater than the cross-section calculated by Egerton (1986). This is inconsistent with an alternative estimate for the mean impact parameter, i.e. $\langle b \rangle = \sqrt{(\sigma/\pi)}$, based on a hard sphere model. The estimate for b' (Howie 1978) derived from the uncertainty principle relies on an indirect argument, which actually depends on the binding energy and extension of the ground state wave function. b' differs from the classical impact parameter, b, used by Rutherford.

The expectation value for the classical parameter, $\langle b \rangle$, can be obtained more directly by the impact parameter method (Bourdillon 1984). It is illustrative to compare values for $\langle b \rangle$ at high or low q.

At *high* q and sufficiently high energy loss, E, the spectrum is dominated by the Bethe ridge (Bethe 1930), a section of which, measured at a fixed scattering angle, appears as a peak in the Compton profile. In this case the small value of b that applies makes it possible

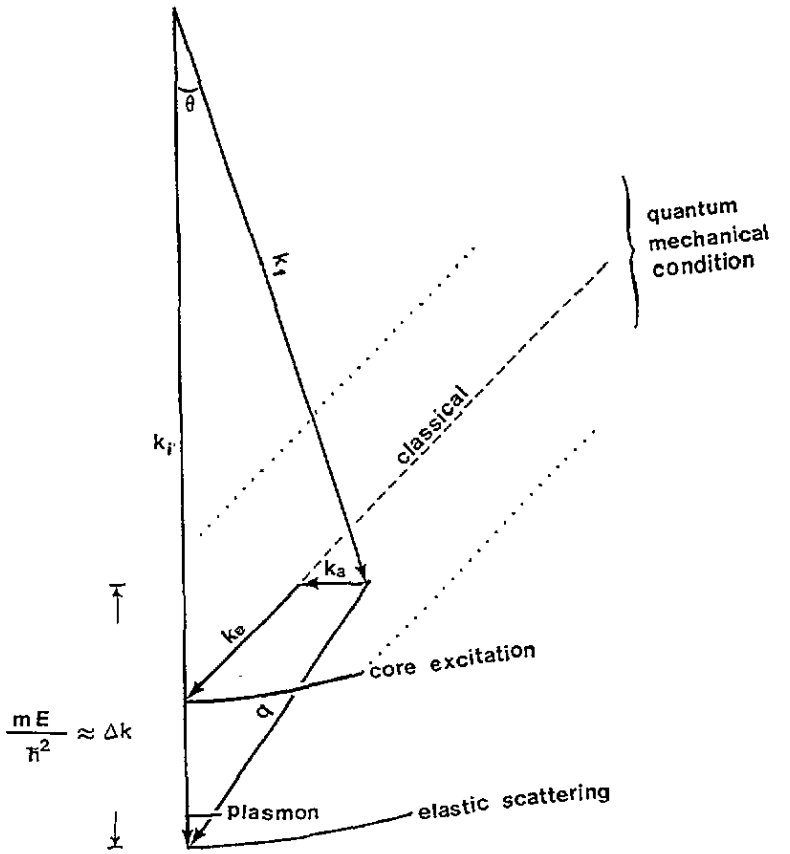

Figure 1. A momentum diagram illustrating the scattering of a fast incident electron with wavevector k_i and scattering vector q to a final state k_f. In typical losses, for which $k_i/\Delta k \sim 200$, the ordinate scale is approximately proportional to energy loss and the abscissa scale to scattering angle. In an event with relatively large scattering angle, the momentum of an ionized electron is $\hbar k_e$ (parallel to the classical condition) and $\hbar k_a$ is the momentum transfer equal to atomic recoil.

to measure the ground state momenta (i.e. the distribution of $\hbar k_a$) through the reciprocal form factor (Bourdillon *et al* 1987). The dependence of q on b is semi-classical, i.e. as in Bohr (1913) but modified by $\hbar k_a$ as illustrated in figure 1. Then $\theta \approx \hbar k_e/(\sqrt{2}\hbar k_i)$ at known E, corresponding to $b \approx 1/(\theta a_0 k_i^2)$.

At *low* q, close to the threshold, $\hbar k_a \gg \hbar k_e$. We suppose that a classical value for the impact parameter can be derived from free-electron scattering, where the scattering angle is now determined from $\theta \approx \hbar k_a/(\hbar k_i)$ corresponding to $b \approx 1/(\theta a_0 k_i^2)$. Then, typically, $b \ll b'$. A clear concept of b is required to explain inelastic scattering of electrons in wedge foils.

3. Inelastic scattering of channelled electrons

Contrast due to electron interactions in foils observed in TEM is understood through the application of kinematical theory or dynamical theory (Howie 1978). Thickness fringes

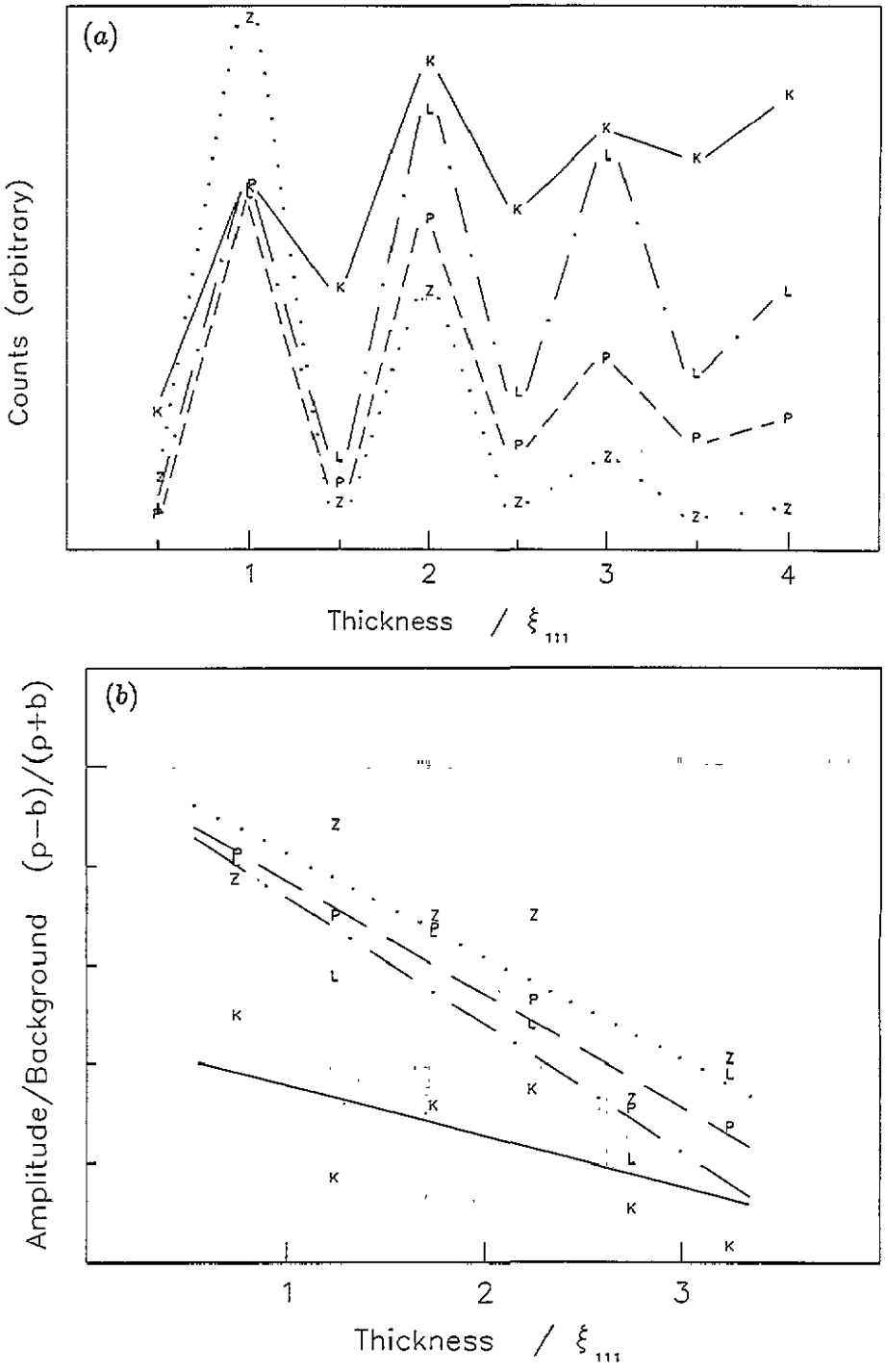

Figure 2. (*a*) The specimen thickness dependence of Al zero (·····, 0 eV), plasmon (– – –, 8–60 eV), L shell (— · —, 73–173 eV) and K shell (——, 1560–1760 eV) losses as a function of thickness at the Bragg angle demonstrating the change in elastic scattering behaviour of the loss electrons with various E. (*b*) The ratio of the amplitude of thickness fringes to background for the energy losses shown in (*a*), plotted as a function of specimen thickness. Straight lines show least-squares fits.

observed in oriented wedge foils show, at the exit surface, the result of pendulum oscillations in bright-field or dark-field images. Figure 2(a) shows four signals observed in bright field from a wedge foil of Al oriented to the [111] Bragg condition. The specimen was prepared by electropolishing immediately before observation, so that the thin oxide film had negligible effect on the signals compared. The signals were observed with an electron energy loss spectrometer using a 100 kV incident beam in a Philips EM400 electron microscope and a collection semi-angle, $\beta \approx 6$ mrad. This angle is similar to the characteristic inelastic scattering angle for K shell electrons in Al ($\theta_E^K = 7.5$ mrad) but considerably larger than the characteristic angles for L shell electrons and plasmons. The signal intensities plotted in figure 2(a) were integrated over energy windows 10 eV wide for the zero-loss peak (Z), over 8–60 eV for the plasmon loss (P) and, after $E^{-\gamma}$ type background subtraction, over windows of 100 and 200 eV for the L and K shell ionizations respectively (L and K). γ is a fitted constant. The lines shown in figure 2(a) are guides to the eye and the peak heights are normalized at one thickness fringe except for the zero-loss intensity, for which the scale is arbitrary. Intensity oscillations are observed at thicknesses up to four extinction distances, $4\xi_{111}$. The core losses both show an increase in intensity up to ξ_{111}, with decreasing amplitude of oscillation on a stable plateau at increasing specimen thickness. The plasmon loss and zero loss show also decreasing amplitude on a background that falls as a result of several features. These include (i) high-order and high-index elastic scattering, which causes electrons to fall outside the microscope objective aperture that defines the collection angle for the spectrometer, (ii) absorption and (iii) thermal diffuse scattering. The large angle elastic scattering likewise explains the former plateaux. To represent the scale of interference causing the pendulum oscillations, the amplitudes of oscillation $[(p-b)/2]$ are normalized against respective backgrounds $[(p+b)/2]$. Figure 2(b) shows the ratios of amplitude/background intensities of adjacent points in figure 2(a). Data fitting was performed by the method of least squares. Notice that after this procedure the Z, P and L intensities have similar intercepts and slopes, but that the intercept and slope of relatively high-loss K have values about half of the corresponding values for Z, P and L. We now consider reasons for the differences and similarities between the four traces in figure 2(a).

An extinction distance in Al of $\xi_{111} = 55.6$ nm (Hirsch *et al* 1977) corresponds to a difference in wavevector at the two dispersion surfaces of $\Delta k = 2\pi/\xi_{111} = 1.1 \times 10^8$, which is three orders of magnitude less than the expectation value of $\langle k^2 \rangle^{1/2}$ for a ground state K shell electron. The difference is reduced to two orders of magnitude for L shell ionization, but Δk is still comparatively small. In the inelastic collisions, therefore, momentum conservation allows ready transitions between dispersion bands. Since thickness fringes arise from interference between waves on the separate dispersion curves, it was therefore surprising to observe the distinct fringes in the P, L and K losses. It is all the more surprising since the energy losses occur throughout the foil, whereas the fringes observed in zero loss are the result of interference of the elastically scattered waves at the base of the foil.

On the other hand, the above treatment of impact parameters shows that (using two beams for simplification) the Bloch wave with the longer wavevector $\boldsymbol{k}^2$, whose amplitude maximizes on atomic planes, interacts more strongly with the core electrons than the wave with vector $\boldsymbol{k}^1$, whose minima occur on atomic planes (Hirsch *et al* 1977). The wave $\boldsymbol{k}^2$ will therefore excite core losses more readily than the wave $\boldsymbol{k}^1$. However, since plasmons extend between atomic planes, P losses should result more or less equally from interactions with both $\boldsymbol{k}^2$ and $\boldsymbol{k}^1$ waves. In contrast, the thickness fringes observed in the P loss are about as distinct as the L loss fringes. This implies that the inelastic scattering is predominantly intraband.

The data suggest further that a single Coulomb impulse, in an inelastic collision, causes

a change in direction of the fast electron, without shifting the k^2 wave from atomic planes to interatomic planes, occupied principally by the k^1 wave. The directional change, typically θ_E, is much larger for the K loss than for the L or P losses and seems to be the main reason for the reduced amplitude, relative to background, of the thickness fringes observed through K loss (figures 2(*a*) and (*b*)). The reduced amplitude occurs because extinction distances increase with specimen tilt away from the Bragg condition so that when $\theta_E \approx \theta_B$, the Bragg angle, and $\theta_E \approx \beta$, there will be some smearing of fringes as observed in K loss. The changes of slope and intercept of the fitted lines in figure 2(*b*) are those predicted in a beam distributed over angles between zero and one Bragg angle.

4. Conclusion

This analysis is consistent with our previously reported experimental findings (Bourdillon 1984, Bourdillon and Williams 1982). There, values for impact parameters in ionization events were used to calculate interactions with Bloch waves excited as described by dynamical theory. Impact parameters were calculated, with cut-off values $R_c \approx R_0$, in the probability distributions for a transition rate in strong coupling (Seaton 1962) $\langle b \rangle = [\frac{1}{3}\pi R_c^2 P(R_c) + \int_{R_c}^{\infty} 2\pi r^2 P(r)\,dr\}/[\frac{1}{2}\pi R_c P(R_c) + \int_{R_c}^{\infty} 2\pi r P(r)\,dr]$, where R_0 is the corresponding mean shell radius of the ground core state. Since R_0 is inversely dependent on $\hbar k_a$ through the uncertainty principle, the results are similar to the more detailed analysis of impact parameters provided in figure 1. The model clarifies the application of classical impact parameters to electron scattering with energy losses either far from the threshold at large scattering angle (when $k_e \gg k_a$, as in Compton scattering) or close to the threshold (when $k_a \gg k_e$). Thickness fringes observed by inelastic scattering in wedge foils can be interpreted by means of Bloch waves in which the wavevectors, in spite of shortening during core ionization, preserve their spatial differentiation in corresponding dispersion bands. The inelastic collisions, even for Al K shell losses, are thus intraband transitions.

References

Ben-Itzhak I, Ashok J and Weaver O L 1993 Impact parameter dependence of classical capture probability from any initial state by fast bare projectiles *J. Phys. B: At. Mol. Opt. Phys.* **26** 1711–26

Bethe H 1930 Theory of the passage of fast corpuscular rays through matter *Ann. Phys., Paris* **5** 325–400

Bethe H and Jackiw R W 1968 *Intermediate Quantum Mechanics* 2nd edn (New York: Benjamin)

Bohr N 1913 On the theory of the decrease of velocity of moving electrified particles on passing through matter *Phil. Mag.* **25** 10–31

Borrmann G 1941 Über Extinktionsdiagramme von Quartz *Z. Phys.* **42** 157–62

Bourdillon A J 1984 The measurement of impact parameters by crystallographic orientation effects in electron scattering *Phil. Mag.* A **50** 839–48

Bourdillon A J, Brydson R D and Williams B G 1987 Electron Compton scattering from beryllium and graphite using parallel detection *J. Microsc.* **145** 293–300

Bourdillon A J, Self P G and Stobbs W M 1981 Crystallographic orientation effects in energy-dispersive x-ray analysis *Phil. Mag.* A **44** 1335–50

Bourdillon A J and Williams B G 1982 Electron energy-loss spectroscopy used For localized Compton scattering *Proc. EMSA (Washington, 1982)* ed G W Bailey (Baton Rouge, FL: Claitor) pp 506–11

Burgess A and Sheorey V B 1974 Electron impact excitation of the resonance lines of alkali metal positive ions *J. Phys. B: At. Mol. Phys.* **7** 2403–16

Burgess A and Tully J A 1978 On the Bethe approximation *J. Phys. B: At. Mol. Phys.* **11** 4271–82

Celiberto R and Rescigno T N 1993, Dependence of electron-impact excitation cross-sections on the initial vibrational quantum number in H_2 and D_2 molecules—X(1)sigma-G+ → B(1)sigma-U+ and X(1)sigma-G+ → C(1)pi-U transitions *Phys. Rev.* A **47** 1939–45

Cherns D, Howie A and Jacobs M H 1973 Characteristic x-ray production in thin crystals *Z. Naturf.* a **28** 565–71

Doyle P A and Turner P S 1968 Relativistic Hartree–Fock x-ray and electron scattering factors *Acta Crystallogr.* A **24** 390–7

Egerton R F 1986 *Electron Energy-loss Spectroscopy in the Electron Microscope* (New York: Plenum)

Geiger J 1962 Zur Streung von Electronen am Einzelatom *Electron Microscopy* vol I, ed S S Breese (New York: Academic)

Hall C R 1966 On the production of characteristic x-rays *Proc. R. Soc.* A **295** 140–50

Hirsch P, Howie A, Nicholson R B, Pashley D W, Whelan M J 1977 *Electron Microscopy of Thin Crystals* (New York: Kreiger)

Howie A 1963 Inelastic scattering of electrons by crystals I. The theory of small-angle inelastic scattering *Proc. R. Soc.* A **271** 268–87

—— 1978 *Diffraction and Imaging Techniques in Material Science* ed S Amelinckz, R Gevers and J van Landuyt (Amsterdam: Elsevier–North-Holland) p 457

Inokuti M 1971 Inelastic collisions of fast charged particles by atoms and molecules—the Bethe theory revisited *Rev. Mod. Phys.* **43** 297–347; addenda, *Rev. Mod. Phys.* **50** 23–6

Reimer L R 1984 *Transmission Electron Microscopy* (Berlin: Springer)

Ricz S, Sulik B and Stolterfoht N 1993 Semiclassical treatment of two-center electron–electron interactions in energetic atomic collision screening effects *Phys. Rev.* A **47** 1930–8

Saldin D K and Rez P 1987 The theory of the excitation of atomic inner-shells in crystals by fast electrons *Phil. Mag.* B **55** 481–9

Schiff L I 1968 *Quantum Mechanics* (New York: McGraw-Hill)

Seaton M J 1962 The impact parameter method for electron excitation of optically allowed atomic transitions *Proc. Phys. Soc.* **79** 1105–12